Journal of Materials Chemistry A

Accepted Manuscript

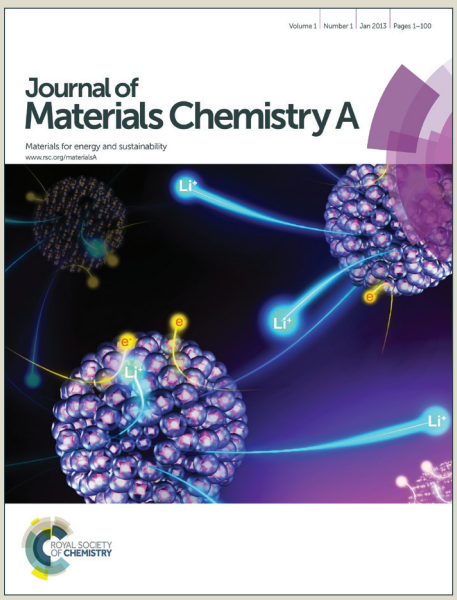

ROYAL SOCIETY OF CHEMISTRY

www.rsc.org/materialsA

Effects of the La/W ratio and doping on the structure, defect structure, stability and functional properties of proton-conducting lanthanum tungstate $La_{28-x}W_{4+x}O_{54+\delta}$. A review.

Anna Magrasó*, Reidar Haugsrud

Department of Chemistry, University of Oslo, Centre for Materials Science and Nanotechnology (SMN), FERMiO, Gaustadalléen 21, NO-0349, Oslo, Norway

* Corresponding author: Dr. Anna Magrasó. E-mail: a.m.sola@smn.uio.no, Telephone: +47-22840660, Fax: +47-22840651

Abstract

The present review focuses on characteristics of lanthanum tungstate in the compositional region 25-30 mol-% La_2O_3 in the La_2O_3-WO_3 phase diagram. These tungstates represent an interesting family of materials for technological applications being proton or mixed proton-electron conductors depending on conditions. The material family was traditionally identified as Ln_6WO_{12}. However, recent efforts have shown that lanthanum tungstate can more correctly be represented by the formula $La_{28-x}W_{4+x}O_{54+\delta}$, where nearly one tungsten (x~1) dissolves in lanthanum sites to form a stable composition. In the present contribution, the importance of the crystal structure and effect of the La/W ratio on stability, defect chemistry and, accordingly, transport properties of this material, are reviewed. A revisited phase diagram in this compositional region is presented. Reported doping strategies on both the A- and B-sites are discussed in view of the applicability of these materials as dense ceramic H_2 separation membranes.

1. Stoichiometry, chemical formula, and phase diagram

Early work on rare-earth tungstates ("Ln_6WO_{12}") was carried out in the 60s and 70s by various researchers [1,2,3,4,5,6,7,8,9],where the chemical formula originated from an older nomenclature expressing the proportion of the parent oxides, i.e. Ln_2O_3:WO_3 = 3:1. This nomenclature has also been widely used for isostructural materials, such as rhenates, uranates and molybdates, generally written as Ln_6MO_{12}, where Ln is a rare earth element or Y, and M = Mo, U or Re [1,10,11,12]. This has clearly led to confusion regarding the actual chemical formula of lanthanum tungstate (and likely for other tungstates with large rare-earth

cations), and to an incorrect range in the La/W ratio with single phase compositions, as argued in the following. Some researchers initially claimed that "La_6WO_{12}" was single phase after annealing powders prepared by traditional solid state reaction at ~1400 °C [8]. However, when Chang and Phillips [7] indexed the XRD patterns of "La_6WO_{12}" according to a fluorite-related structure, two additional reflections were present, more recently identified as La_2O_3 [13]. Yoshimura and Rouanet [9] studied the phase diagram of the La_2O_3-WO_3 system in more detail based on rapid quenching of oxide melts (see **Figure 1a**, re-drawn by Chambrier *et al.* [14]). They observed that La_6WO_{12} is not thermodynamically stable below 1740 °C [9,15], but rather that a more tungsten rich phase, $La_{10}W_2O_{21}$ (also written as La_2O_3:WO_3 = 5:2), forms below this temperature. Due to the numerous ways of reporting the chemical formula of lanthanum tungstate (summarized in **Table 1**) it is convenient to use the La/W ratio to avoid misperception, as they all refer to the same material with small variations in the cation ratio. The compositions will be labeled as LWOx, where x represents the nominal La/W ratio multiplied by 10.

Recently, Magrasó *et al.* [13] have shown that neither LWO60 ("La_6WO_{12}") nor LWO50 ("$La_{10}W_2O_{21}$") are single phase after firing freeze dried powders at temperatures in the range 1300-1500 °C: In addition to the fluorite-related material forming for both compositions, La/W=6 yields La_2O_3 segregation while for La/W=5, a W-rich phase identified as $La_6W_2O_{15}$ was formed. Later, other laboratories have independently confirmed that LWO60 and LWO50 are not single phase also when using conventional solid state synthesis methods [16,17] at temperatures below 1500-1600 °C. Recently [18], it was stated that the previous chemical formulas considered to be two different compositions ("La_6WO_{12}" or "$La_{10}W_2O_{21}$"), indeed refer to the same material (both containing segregations), and may be seen as a simplification of a more complex formula: $La_{28-x}W_{4+x}O_{54+3x/2}$ (LWO) [19]. Indeed, the powder data files available for "La_6WO_{12}" (pdf: 30-0687, a=11.179 Å) and "$La_{10}W_2O_{21}$" (pdf: 30-0686, a= 11.167 Å) reveal that the number of reflections and their intensities are essentially equal, with only a small difference in the lattice parameters.

From the data available in ref. [13], a new phase diagram was constructed in the region 6≥La/W≥4.8 (**Fig. 1b**) at temperatures of 1000-1600 °C. Important to note from this diagram is firstly that there is a continuous solid solution where the cubic fluorite-related phase ($La_{28-x}W_{4+x}O_{54+3x/2}$, x~1) is identified. This can be concluded since there are no

apparent differences in the number of peaks (from XRD) or their relative intensity, meanwhile the lattice parameter changes continuously as a function of La/W ratio (**Figure 2**). Secondly, the composition range where LWO is single phase depends on temperature. This reflects that the solubility of tungsten in La2 sites (x in $La_{28-x}W_{4+x}O_{54+3x/2}$) varies with temperature. Thirdly, if the solid solubility range is hypothetically extrapolated to temperatures above 1600 °C (dotted lines in **Fig. 1b**) the composition written by Yoshimura [9] as "La_6WO_{12}", reported to be stable above 1740 °C, indeed falls inside the single phase region. It is interesting to note from the phase diagram reported by Yoshimura and Rouanet (c.f. **Fig. 1a**) [9] that the two undefined high temperature regions present around $La_{10}W_2O_{21}$ and La_6WO_{12} correspond to one single solid solution region, as drawn in **Fig. 1b**.

Figure 2 shows the variation of the lattice parameter as a function of the nominal La/W ratio derived from XRD after firing the different compositions at 1300, 1400 or 1500 °C. As reported earlier [13], there are three distinguishable regions. In *region I* (low La/W ratio) and *region III* (high La/W ratio) the lattice parameter is virtually independent of the La/W ratio (though dependent on firing temperature), and XRD patterns show segregation of $La_6W_2O_{15}$ or La_2O_3 phases, respectively. In *region II* the patterns show only single phase and the lattice parameters increase with increasing lanthanum content, following a linear behavior. The La/W-composition range of *region II* depends on firing temperature, well in accordance with the phase diagram in **Fig. 1b**: At lower firing temperatures, the lattice parameters level off at lower values, which indicates that the LWO phase contains a lower La/W ratio compared to for higher temperatures. At 1500 °C, LWO is single phase for 5.7 ≥La/W≥ 5.3, and the interval narrows down with decreasing final temperature (e.g. 5.4 ≥La/W≥ 5.2 at 1300 °C).

2. The crystal structure of lanthanum tungstate

Reports indexing X-ray diffraction patterns of the tungstates with larger lanthanide cations have existed since the 60s and 70s [6,7,20,21,22,23] but these studies did not present complete structural details (e.g. atomic positions). One of the inconsistencies with the traditionally written formula La_6WO_{12} realized recently [13] was the density of the material. The density of sintered, single-phased powders was measured by He-pycnometry to be essentially independent of composition and equal to ~6.3-6.4 g/cm^3 (see **Table 2**) [13]. With

the stoichiometry "La_6WO_{12}" (Z=4, i.e. $La_{24}W_4O_{48}$) and the cell parameter (a~11.19 Å), the density can be calculated to be 5.75 g/cm^3. This is significantly lower than the experimental density from powders, and unequivocally implies that the unit cell contain more ions than 24 lanthanums, 4 tungstens and 48 oxygens. Taking the cation content of a cell into account, a structural model for lanthanum tungstate was put forward using the space group $F\bar{4}3m$ [13] where lanthanum occupies 2 different Wyckoff positions, La1 and La2. La1 resides in *4a* (0, 0, 0) sites, with full occupancy, while La2 sits on *24f* (¼, ¼, ¼) positions, close to full occupancy. Tungsten is in position *4b* (½, ½, ½). All the oxygen is placed in *16e* sites (*x*, *x*, *x*) with x ~0.13 and x ~0.87. A follow up study suggested that X-ray and neutron powder diffraction data can be indexed using either $F\bar{4}3m$ or $Fm\bar{3}m$ cubic cells, with only minor differences between the two [18]. It is important to emphasize that the thermal factors for La2 and O2 were quite high using both these models, which indicated disorder in the respective sublattices.

Later high resolution X-ray synchrotron studies [19] revealed a very small distortion from the cubic cell, below the detection limit of a conventional laboratory X-ray diffractometer. Anyhow, the synchrotron data confirmed the atomic positions of the structural model (La1 in *4a*, La2 in *24f*, W1 in *4b*, and O1-O2 in *16e* sites) reported in [13]. The stoichiometry in this case (and also when using $F\bar{4}3m$ or $Fm\bar{3}m$ s.g.) would render $La_{28}W_4O_{54}$ (La/W=7), which leads to a La/W ratio higher than the one measured experimentally (La/W~5.3-5.7). Consequently, other tungsten positions must exist in the structure. Density Functional Theory (DFT) predicted that W dissolves in La2 sites to form a stable compound [19], so the "additional" tungsten positions were located. The atomic arrangements of two "ideal" compositions from DFT calculations, $La_{28-x}W_{4+x}O_{54+\delta}v_{2-\delta}$ for x=0 and 1, are drawn in **Figure 3**. These correspond to $La_{28}W_4O_{54}v_2$ (La/W=7, LWO70, x=0), and $La_{27}W_5O_{55.5}v_{0.5}$ (La/W=5.4, LWO54, x=1). From the models in **Fig. 3**, it is clear that the structure of lanthanum tungstate at the local scale is complex: There is disorder on the oxygen sublattice [18] and static disorder of the La2 site [24]. The disorder rationalizes the high and anisotropic thermal factors of the O2 and La2 sites mentioned earlier.

Further insight of the local atomic arrangements in lanthanum tungstate (LWO54) has been obtained from the combination of atomic pair distribution function analysis (PDF) of time-of-flight neutron and synchrotron X-ray data with the models from DFT [25]. These

experimental data verified the presence of W on the La2 site as suggested from DFT (**Fig. 3**) [19] and revealed that these calculations led to a plausible model to describe the experimental data of this complex oxide. Another work elucidated a local model combining synchrotron X-ray PDF analysis and EXAFS [24]. They reported that the structure of LWO54 can be described by an average model (cubic fluorite supercell; space group $Pa\bar{3}$) with disorder in the oxygen and La2 sublattice. To describe the static disorder of the La2 site, the authors in [24] use the space group $Pa\bar{3}$ (instead of $F\bar{4}3m$ or $Fm\bar{3}m$). Nevertheless, these two final models in refs [24, 25] are in good agreement with each other. It is important to highlight that the latter [24] detected experimentally ~4.4% of anti-site disorder on the La2 site, thus confirming the dissolution of W on La2 sites predicted earlier from DFT calculations (1/24: ~4.2%) [19,25].

One important outcome of the structural model presented in **Fig. 3** is the overall stoichiometry: $La_{28-x}W_{4+x}O_{54+\delta}v_{2-\delta}$ (δ=3x/2). From this formula, it is straightforward to deduce the variation in number of vacancies with the lanthanum-to-tungsten ratio and some examples are given in **Table 3**. There are 2 vacancies per formula unit in the "stoichiometric" composition (LWO70). However, to reduce the number of vacancies to about ½ per unit cell and stabilize the structure, approximately one W is accommodated in La2 sites per formula unit as a donor dopant, $W_{La}^{\bullet\bullet\bullet}$. LWO54 is accordingly a stable composition [19]. In other words, lanthanum tungstate is a nominally undoped material with an inherently deficient oxygen sublattice where the concentration of vacancies depends directly on the La/W ratio (and final sintering temperature) (see **Table 3**). This can be related to the phase diagram in **Fig. 1b**: the temperature dependence of the LWO phase likely reflects the temperature dependence of the solubility of W in the La2 site.

There is one example in the literature that reports a stable composition with a cation ratio 7-to-1 that is comparable to the lanthanum tungstate: $Y_7ReO_{14-\delta}$ (with δ~0; $Y_{28}Re_4O_{56}v_{\sim 0}$) [26]. The main difference between $La_{28}W_4O_{54}v_2$ and $Y_{28}Re_4O_{56}v_{\sim 0}$ is the vacancy concentration, related to the oxidation state of W(VI) and Re(VII). Rhenium will most probably not dissolve in yttrium sites because there are no more vacancies which can compensate a possible donor in the lattice, while tungsten dissolves in La2 sites to reduce the vacancy concentration from 2 to ~1/2 per unit cell.

3. The compositional stability of LWO

Figure 4 depicts the variation of the conductivity for different lanthanum tungstates with time at 1100 °C in wet H_2: For LWO53 and LWO54 the conductivity remains essentially constant and stable, while it degrades rapidly for LWO56 and LWO57. This behavior may be rationalized by the thermodynamic stability of the phase (**Fig. 1b**). At 1100 °C, the diagram shows that LWO54 and LWO53 are single phase materials, while LWO56 and LWO57 are not. Although all these compositions are single phase after sintering (1500 °C), the cations will reorganize at lower temperatures toward the stable composition with a lower La/W ratio than in LWO56 and LWO57 and therefore La_2O_3 is segregated at 1100 °C. One could, in principle, expect that the conductivity of LWO57/LWO56 levels off at the same value as LWO54, but it continues to decrease. This may be associated with the formation of La_2O_3, possibly segregating to the grain boundaries, decreasing the total conductivity.

To further elucidate the origin of this degradation in conductivity, the dependence of the conductivity on pO_2 at 1000 °C for LWO53 and LWO57 was determined before and after long term annealing at 1100 °C (**Fig. 5**): The LWO53 data is unaltered, while for LWO57 the heat treatment induces a significant decrease in the ionic, pO_2 independent, plateau in conductivity at intermediate oxygen pressures. XRD confirmed that La_2O_3 segregations can be found after measurements shown in **Fig. 4** for LWO57/LWO56, while these are absent in LWO54/LWO53 (**Fig 6**). The lattice parameter of the nominal LWO56 decreases from 11.187 Å to 11.175 Å (in accordance with the latter being richer in tungsten cf. **Fig. 2**), whereas the lattice parameter of LWO54 remains essentially constant before and after the treatment (11.176 Å and 11.178 Å, respectively). These gradual changes encountered for the LWO56 and LWO57 with time altogether reflect the relative increase in the number of W donors at the La2 site followed by a decrease in oxygen vacancy concentration. This behavior is attributed to the higher stability of the crystal structure with low concentration of vacancies at lower temperatures. There is, therefore, a trade-of between high ionic conductivity and stability where LWO54 probably is the best compromise.

It is worth to mention that there is no visible effect of La/W ratio on the microstructure of the materials [13]. The average grain size of powders prepared from freeze-

dried precursors increases from 1–3 μm (1400 °C), 3–10 μm (1500 °C) to 10–30 μm (1600 °C) independent of composition. The densification properties and variation of particle size of the different LWO compositions do not differ significantly, even for those containing segregations of either La- or W-rich phases [13].

4. Defect structure in LWO and hydration thermodynamics

The effect of oxygen partial pressure on the conductivity of LWO for various La/W ratios is shown in **Figure 7**. The flat regime at intermediate oxygen partial pressures represents ionic conductivity, while the contributions at either side represent n- and p-type electronic conductivities, in accordance with previous studies [27,28]. The overall conductivity behavior of LWO56, LWO57 and LWO60 is rather similar. This reflects that the level of lanthanum in the structure is saturated and therefore the maximum number of vacancies has been reached. It is evident that below La/W=5.6, the ionic conductivity decreases monotonically with decreasing La/W ratios (see the pO_2 independent plateau in **Fig. 7**), and is roughly proportional to the concentration of vacancies according to $La_{28-x}W_{4+x}O_{54+\delta}v_{2-\delta}$. This is further illustrated in **Fig. 8** displaying the ionic conductivity at 800 °C. The difference in ionic conductivity between LWO56 and LWO52 is approximately one order of magnitude, as shown by the temperature dependence in wet Ar (**Figure 9**). Overall, this behavior supports the hypothesis that W on La site (x) acts as a donor, ($W_{La}^{\bullet\bullet\bullet\bullet}$), and is mainly compensated by oxide ions filling up the oxygen vacancies (v). Consequently, tungsten reduces the ionic conductivity due to a decrease in concentration of oxygen vacancies, as reported by Erdal *et al.* [29]. The positive donors also increase the concentration of electrons which rationalizes the somewhat higher relative contribution of n-type conductivity in LWO53 than in LWO57. Electrons remain in minority concentration-wise, but with higher mobility they still have a tangible effect on the total conductivity. The ionic conductivity in LWO has been calculated based on the defect model described in [30], using the concentration of vacancies from **Table 3** for each LWO composition within the single phase region. The calculated conductivities at 800 °C are in accordance with the experimental ones (c.f. **Fig. 8**), supporting the present defect model.

The effect of water vapour partial pressure (pH_2O) at constant pO_2 on the conductivity of LWO57 and LWO53 is shown in **Figure 10**. The conductivity increases with increasing

$p\mathrm{H_2O}$, and the dependence increases with decreasing temperature. This reflects that the concentration of protons and, accordingly, their contribution to the total conductivity, increases with decreasing temperature and increasing water vapor pressure, in accordance with the exothermic hydration reaction:

Equation 1 $$\mathrm{H_2O + v_O^{\bullet\bullet} + O_O^x = 2OH_O^\bullet}$$

This reaction is, however, only strictly correct for materials with doubly charged oxygen vacancies, typically the result of acceptor doping. LWO, on the other hand, has inherent vacancies with partial occupancy. Norby [31] has derived a Kröger-Vink compatible notation for defects in inherently defective sublattices, and Erdal *et al.* [29] applied this approach to LWO. Hydration of $\mathrm{La_{28-x}W_{4+x}O_{54+\delta}v_{2-\delta}}$ can accordingly be written:

Equation 2 $$\mathrm{H_2O(g) + O_{\frac{56}{54}O}^{\frac{4}{56}\prime} + v_{\frac{54}{56}O}^{\frac{108}{56}\bullet} = 2\ OH_{\frac{54}{56}O}^{\frac{52}{56}\bullet}}$$

and the electroneutrality condition is expressed:

Equation 3 $$3\left[W_{La}^{\bullet\bullet\bullet}\right] + \frac{108}{56}\left[v_{\frac{54}{56}O}^{\frac{108}{56}\bullet}\right] + \frac{52}{56}\left[OH_{\frac{54}{56}O}^{\frac{52}{56}\bullet}\right] = \frac{4}{56}\left[O_{\frac{54}{56}O}^{\frac{4}{56}\prime}\right]$$

The reader is referred to refs [29,31] for details on the derivation. From this model, the hydration and the ionic conduction can be rationalized. The effective charges of the vacancies (~1.93) and the protons (~0.93) are very close to those of a standard acceptor-doped system (2 and 1, respectively), so lanthanum tungstate behaves, in practice, as if it was effectively acceptor doped. As outlined above, electrons and electron holes are not significant concentration-wise in the present experimental window and contribute to the conductivity of lanthanum tungstate as minority defects (at relatively high temperatures) only. The simplified electroneutrality condition (*Eq. 3*) accordingly takes only ionic defects into account.

Now comparing the behaviour of the different tungstates in **Fig. 10**, we observe that there is essentially no difference in the water vapor dependency of the conductivity of LWO57 and LWO53, which confirms that the defect chemical model is the same for both materials. The conductivity of LWO57 is higher than LWO53, as expected from the higher

vacancy concentration in the dry state and higher concentration of protons upon hydration at intermediate and low temperatures. The conductivity is close to being proportional to $pH_2O^{1/3}$ at the lowest temperature, which was initially speculated to be related to the hydration of oxygen interstitials in LWO [28,32]. Later investigations of the hydration of lanthanum tungstate by means of thermogravimetry [33] revealed that the dependency of the proton concentration is essentially proportional to $pH_2O^{½}$ at relatively high temperature, in accordance with the defect chemical model from *equation 3*. This behavior is typical for the exothermic hydration of oxygen vacancies generally encountered in acceptor doped systems and shows that LWO indeed behaves as though it was nominally acceptor doped. From the TG data, one finds that LWO53 hydrates up to a level corresponding to the oxygen vacancy content from **Table 3**, in line with the crystal structure derived by Magrasó *et al.* [19]. LWO56, however, hydrates only 66 % of the nominal vacancies. There are several possible reasons for this discrepancy: As demonstrated earlier in this contribution, compositions with high lanthanum contents are thermodynamically unstable at lower temperatures (typically below 1200 °C), forming LWO54 and a La_2O_3 secondary phase. As part of this process, the number of oxygen vacancies potentially available for hydration decreases. Consequently, the maximum level of hydration for LWO56 will be sensitive to thermal history and treatments like the drying procedure at 1000-1100 °C performed in [33] before the actual hydration experiment. In this respect, it is interesting to note that the maximum level of hydration reached for LWO56 corresponds essentially to a fully hydrated LWO54 composition [33]. An alternative interpretation to the low hydration level in the LWO56 composition that cannot be entirely ruled out is that vacancy ordering in the compositions with higher vacancy concentration seen by TEM [19] may inhibit hydration in LWO56.

5. Effects of A-site doping in LWO

Iso-valent substitution. Haugsrud [28] reported that the protonic conductivity of a series of tungstates "Ln_6WO_{12}" decreases in the order La>Nd>Gd>Er, likely related to a decrease in crystal symmetry towards the smaller rare-earth [5]. The conductivity of all these materials is dominated by protons under wet atmospheres below 900 °C. The maximum in proton conductivity is observed for nominally undoped "La_6WO_{12}" in the order of $3–5\cdot10^{-3}$ S/cm. "Nd_6WO_{12}" exhibits higher p-type conductivity and lower protonic conductivity compared to the lanthanum counterpart. Escolastico *et al.* [34] reported later that the protonic

conductivity of La-substituted "Nd_6WO_{12}" is higher for the composition with more La, in line with the studies by Haugsrud [28]. Partial substitution of Y by La [16] lowered the overall electrical conductivity. The effect of Y is likely related to a decrease in crystal symmetry and to an ordering of the vacancies in the lattice as reported by Diot *et al.* [35], reducing the mobility of protons and oxygen vacancies.

Donor-doping. Shimura *et al.* [27] showed that partial substitution of Zr for La decreases the conductivity. Zr is probably substituting lanthanum, acting as a donor dopant ($Zr_{La}^{\bullet}$) which reduces the concentration of vacancies, and therefore, the ionic conductivity. Similarly, another study [36] showed that when Ce was replaced by La, the ionic conductivity decreased with increasing cerium content, accompanied by a slight increase in the electronic conductivity under reducing conditions, both demonstrating the donor effect.

Acceptor-doping. Haugsrud [28, 32] also reported that acceptor doping decreased the ionic conductivity for LWO60 when lanthanum was substituted by calcium (0.5 and 5%). This was unexpected, and initially speculated to reflect that acceptor substitution decreased the number of protons incorporated, or slowed down their mobility. It was suggested that the acceptor (Ca^{2+}) traps protons based on the observation that the apparent enthalpy of proton mobility increased upon acceptor doping. The effect of Ba doping also proved to decrease the overall conductivity [37]. In this case, impedance spectroscopy showed that the grain boundaries were orders of magnitude more resistive than the bulk.

Later studies report that there is no detectable difference neither in conductivity nor the crystal structure between LWO56 and 2% Ca-doped LWO56 [18]. In the present contribution, we report that the conductivity actually depends on the thermal history, and further illustrated here in **Fig. 11**, showing the effects of annealing at different temperatures for 2% Ca-doped LWO56. As evident, the conductivity remains essentially stable at 800 °C in wet Ar (representing the ionic conductivity), but decreases over time at 1000 °C (2), and even more rapidly at 1200 °C (3). The level of the conductivity at 800°C also decreases gradually as the annealing time at the higher temperatures increases. Interestingly, however, opposite effects are encountered after annealing at temperatures as high as 1400°C; the conductivity increases during the annealing and also the level at 800°C is higher than the original as-sintered one. This behavior either indicates that LWO phases with different La/W

ratio are stabilized (as the phase diagram in **Fig 1b** suggests) at high temperatures, or that Ca-doping is meta-stable and tends to be expelled at intermediate temperatures between ex-solution and (re)dissolution temperatures. It is important to emphasize that LWO has very low solubility of acceptor dopants (e.g. Ca^{2+}, Sr^{2+}), around 1 mole %, or less. In comparison with other systems, there are a number of ternary or higher oxides in which two cations of different valence are site disordered, and where doping has none or unexpected effects [38]. In those cases, doping results only in shifting the ratio of the two disordered cations, as this may have a much lower energy cost. This is accompanied by the precipitation of a phase or domains rich in the expelled cation, as probably occurs in our case.

Overall, A-site doping in LWO has, so far, been unsuccessful to enhance the conducting properties of the material.

6. Effects of B-site doping in LWO

Acceptor-doping. Nb substitution in LWO was reported to increase the ionic conductivity by acceptor doping on the W-site [39]. The highest conductivity was measured for $La_{27}NbW_4O_{55}$ to be 0.01 S/cm at 800 °C in wet N_2. This is slightly higher than $7{\cdot}10^{-3}$ S/cm (for LWO56) or $4{\cdot}10^{-3}$ S/cm (for LWO54) in wet Ar, at 800 °C. The authors mentioned that these materials are nearly pure ionic conductors at low temperatures, with transport numbers ~0.98 below 800 °C. Replacement of W by Re has also been reported [40]. The conductivity of undoped LWO55 is $\sim 3{\cdot}10^{-3}$ S/cm, and it increases to $\sim 4{\cdot}10^{-3}$ S/cm at 800 °C in wet H_2 when 20% Re substitutes W. The authors report that the conductivity is independent of pO_2 under reducing conditions. This indicates that ionic conductivity dominates under these conditions and that rhenium probably acts as an acceptor dopant. Although both studies [39,40] report effects of water that indicate contribution of protons under wet conditions and intermediate temperatures, the ratio between oxide ion/protonic conductivity has not been determined for any of these substitutions. This should be studied further to evaluate the potential use of these materials in hydrogen technology applications.

Donor-doping. Amsif *et al.* [41] have recently shown that the replacement of tungsten by molybdenum in lanthanum tungstate [$La_{28-y}(W_{1-x}Mo_x)_{4+y}O_{54+\delta}$] is efficient to improve the electronic conductivity substantially without altering the protonic conductivity

significantly, at least up to x=0.4. This affirmation is based on the following experimental data: (i) the ionic conductivity is relatively independent of the Mo content up to 40% substitution, see pO_2 dependencies in **Figure 12**, taken from refs. [30,41]; (ii) the proton/oxide ion conductivity does not seem to be affected by Mo up to 40% substitution, see pH_2O dependencies in refs. [30,41] and the comparison between Mo-free and Mo-containing compositions shown in **Fig. 13**; and (iii) the partial protonic conductivities measured using the EMF method render very similar values for LWO54 and 30% Mo-substituted LWO54 [30]. This implies that Mo substitution in LWO results in an overall increase of the ambipolar proton-electron conductivity, suitable to enhance H_2 permeation in dense ceramic membranes, as also shown by others [40,42]. This is treated in more detail in section 7.

All in all, B-site doping of LWO has proven to be more successful than A-site doping to enhance the conductivity of the materials. Either the ionic or electronic/ambipolar conductivity can be increased depending on the dopant, and will be discussed further in the next section.

7. Discussion. Applicability of the materials.

Lanthanum tungstate and related compositions have during the last years attracted considerable attention as electrolyte materials for proton conducting solid oxide fuel cells (PC-SOFCs) and dense hydrogen gas separation membranes [43]. LWO has the potential of being a suitable proton conducting electrolyte material in the range of 600-700 °C, with proton conductivities in the order of 1 mS/cm. At high temperatures, LWO dehydrates, oxygen vacancies start to form at the expense of protons according to *eq. 1-2*, and oxide ion conductivity starts to dominate over proton conductivity above ~750 °C [28,30]. Therefore, LWO-based PC-SOFCs should operate up to temperatures of about 600 °C, where the electrolyte membrane behaves as a pure proton conductor. Fuel cell testing with ~1 mm thick electrolyte and Pt electrodes has confirmed that LWO is predominantly an ionic conductor. The mediocre power output achieved[30], shows that thin electrolytes (~1 μm) with tailor-made electrodes are required to make LWO-based PC-SOFCs competitive. NiO is not chemically compatible with LWO [44] so Ni-cermet-supports with *in-situ* reduction of sintered NiO-LWO composites are not viable. Serra and co-workers [44,45] tested $LaCrO_3$-

based materials as anodes. The best performance was achieved when $La_{0.75}Ce_{0.1}Sr_{0.15}CrO_{3-\delta}$ was infiltrated with nickel nanoparticles. The overall ASR for this system was 0.3 Ωcm^2 at 750 °C in wet H_2. LWO is chemically and mechanically stable with LSM ($La_{0.7}Sr_{0.3}MnO_{3-\delta}$) and LSCM ($La_{0.75}Sr_{0.25}Cr_{0.5}Mn_{0.5}O_{3-\delta}$) [46], but relatively high ASRs were measured (3-4 $\Omega \cdot cm^2$ in wet air at 750 °C, for LSM-based cathodes [46,47]. Optimized 50% Pr_2NiO_4 – 50% LWO composites show ASR values of only 0.5 $\Omega \cdot cm^2$ at 700 °C, as such being a promising cathode candidate for use in PC-SOFCs [48].

Focus onwards will be on the regime where LWO is a mixed proton-electron conductor. There are increasing number of reports on hydrogen flux over membranes of LWO-based materials, and the potential as hydrogen permeable membrane has thus been demonstrated. For unsubtituted LWO, the electronic conductivity is relatively low at T<800 °C, and the H_2 permeation via ambipolar transport of protons and electrons is low at these temperatures. Even up to ~950-1000 °C, the hydrogen flux is limited by n-type electronic conductivity, whereas protons are the limiting species above this temperature due to the dehydration of the material. At 1000 °C, the ambipolar proton-electron conductivity in lanthanum tungstate (LWO56) is approximately 10^{-3} S/cm [49], which renders hydrogen fluxes comparable to the best mixed proton-electron conducting perovskites. The hydrogen flux of LWO56 is 0.041 ml/min cm^2 (wet H_2 on the feed side) [49], 0.046 ml/min cm^2 for Nd-substituted LWO55 (wet 50% H_2) [34] or ~0.08 ml/min cm^2 for LWO55 (wet 50% H_2) [40], all at 1000 °C and with wet Ar on the permeate side. These membranes were 1-2 mm thick, and the flux can be further increased by decreasing membrane thickness. Gil *et al.* [50] reported that a 25-30 μm LWO56 supported on a porous matrix of the same composition, led to an increased hydrogen flux (0.14 ml/min cm^2 in wet 10 % H_2/Ar). This value was, however, lower than expected based on measurements for thicker membranes, and the deviation may indicate that surface kinetics is limiting the flux across the thinner membrane, as also suggested by the sluggish transport kinetics in LWO56 reported by Hancke *et al.* [51].

It is important to highlight when discussing the application of these materials as hydrogen membranes that the level of H_2 in the permeate increases dramatically when the carrier gas on the permeate side is wetted. This could, in principle, be related to a higher degree of hydration of the membrane, but it has been shown that water splitting is the main cause [42]. Water splits as a consequence of the oxygen gradient from the sweep side to the

feed side and the oxide ions migrate through the membrane towards the feed, leaving H_2 behind at permeate side. This H_2 does consequently not originate from ambipolar transport of protons and electrons from feed to permeate side. This effect becomes more important at the higher temperatures, as the oxide ion conductivity increases with increasing temperature. Although for H_2 separation purposes water splitting does not pose a problem, it is in many cases important to realize how much of the detected H_2 that comes from permeation (representing actual gas separation) and how much that stems from water splitting at the permeate side (hydrogen production, not separation). It has been shown that the hydrogen flux detected when the permeate side is dry is in accordance with the hydrogen flux estimated from ambipolar transport of protons and electrons [42], and can be taken as a reference to differentiate H_2 separation and H_2 production.

The chemical stability of LWO against CO_2 has been confirmed for LWO55 [40]. This represents one of the main advantages of this family of materials over the previous state-of-the-art $SrCeO_3$, which readily forms carbonates even in atmospheres containing small amounts of CO_2. It is also interesting to highlight that LWO is more stable towards cation diffusion-related degradation than many of the most promising oxygen transport membrane materials, since bulk diffusivities of W and La are very similar, and are determined by relatively slow kinetics [52]. The thermal expansion coefficient (TEC) for lanthanum tungstate was determined by different laboratories to be ~$11\text{-}12 \cdot 10^{-6}$ K^{-1} [18,53], and the expansion is isotropic since the crystal symmetry is cubic. It is important from a technological point of view that a material with a practical application exhibits a linear isotropic thermal expansion coefficient, to make thermal compatibility with the surrounding materials easier. In addition, the TEC is essentially independent of pO_2 (LWO does not reduce or oxidize significantly) and only slightly dependent on pH_2O, due to hydration.

As mentioned earlier, B-site doping strategies have been the most successful approach to increase the conductivity in LWO. The replacement of tungsten by molybdenum in lanthanum tungstate is particularly interesting, since the electronic conductivity is enhanced substantially without altering the protonic conductivity significantly [30, 41]. On the other hand, other authors have claimed that Mo substitution decreases protonic conductivity [40]. However, the statement was based on results from measurement of the pH_2O dependency under reducing conditions. Under these conditions electronic conductivity prevails and the

relative contribution of protonic conductivity is smaller for the Mo-substituted LWO, but it does not necessarily mean that the σ_{H^+} is smaller. The influence of electronic defects on the effect of water to the conductivity can be minimized if the dependencies are done under inert or oxidizing conditions, as performed in refs. [30, 41] and **Fig. 12** (all in O_2). We should remind the reader that p-type conductivity is relatively independent of the Mo-content [41], and quite low at the temperatures measured (500-800 °C).

The ambipolar proton-electron conductivity given in Eq. 4:

Equation 4

$$\sigma_{amb} = \frac{\sigma_{H^+} \cdot \sigma_{e'}}{\sigma_{H^+} + \sigma_{e'}}$$

has been estimated for $La_{28-y}(W_{1-x}Mo_x)_{4+y}O_{54+\delta}$ with $0 \leq x \leq 0.4$ and $y \sim 1$ (**Figure 14**). σ_{H^+} is taken from the modeled partial proton conductivity extracted using the EMF method (and assumed constant for $x \leq 0.4$), and $\sigma_{e'}$ is extracted for each composition using the pO_2 dependency of the conductivity from **Figure 12**. The estimated ambipolar conductivity is clearly dependent on the Mo-content at all temperatures, due to the strong enhancement of electronic conductivity with increasing Mo-content. The σ_{amb} is approximately a factor of two higher at 1000 °C when 20% of the W is replaced by Mo. The enhancement is even more evident at the lowest temperatures: already at ~650 °C, the ambipolar conductivity of a 30-40% Mo substitution is comparable to that obtained LWO54 at 1000 °C . This is a considerable improvement and decreases the operating temperature of hydrogen separation membranes compared to LWO. One may note from **Fig. 14** that the temperature dependence of σ_{amb} is steeper for LWO than for the Mo-substituted tungstate. This reflects that the limiting species change from being electrons (in LWO) to protons (in 40% Mo-LWO). Recent permeation measurements comparing LWO with 30% Mo-LWO confirm this statement [42].

When comparing to other state-of –the-art materials for hydrogen permeation, acceptor-doped $SrCeO_3$ is the most studied so far, see e.g. [54,55,56,57,58]. These materials are predominantly protonic conductors below 600–700 °C [54], so that high ambipolar conductivity can only be obtained *via* suitable doping and/or by increasing temperature. Oh *et al.* [58] reported that the ambipolar conductivity of $SrCe_{0.85}Eu_{0.15}O_{3-\delta}$ was close to 10^{-3} S/cm at 900 °C, which is comparable to that of 40% Mo-LWO at 600 °C. The hydrogen flux

measured for 1 mm thick $SrCe_{0.95}Yb_{0.05}O_{3-\delta}$ at 677 °C is ~0.007 ml/cm^{2}min [59], or ~0.05 ml/cm^{2}min for 0.8 mm thick $SrCe_{0.95}Tm_{0.05}O_{3-\delta}$ at 950 °C [60]. The flux can increase substantially with decreasing membrane thickness, as reported for a 33 μm thick $SrCe_{0.7}Zr_{0.2}Eu_{0.1}O_{3-\delta}$ (0.23 ml/cm^{2}min at 900 °C) [61], and for a 2 μm thick $SrCe_{0.95}Yb_{0.05}O_{3-\delta}$ (~15 ml/cm^{2}min at 677 °C) [59]. The main drawback for a widespread practical application of $SrCeO_3$-based materials is the low chemical stability, and the tungstates can offer a feasible alternative with substantially increased chemical stability. The H_2 permeation of a 5 μm-thick 40% Mo-substituted LWO is predicted to be ~2 ml/cm^{2}min at 600 °C, using a gradient of pH_2 of one order of magnitude, an ambipolar conductivity of~$1.6\cdot10^{-3}$ S/cm for, and assuming that bulk diffusion is limiting. We should emphasize, however, that surface limitations have been encountered for LWO and Mo-substituted LWO [42], and that surface treatment to increase kinetics must be taken into account in the optimization process.

All in all, Mo-substituted LWO embraces a family of truly competitive materials for H_2 permeation and further development on the optimization of the cation ratio, microstructure of the membrane and surface treatment will be dealt with in the future.

Acknowledgements

The data reported and the discussion thereof summarizes for a large part work financed by Research Council of Norway (grant nos. 187160, 193816,190901,171157, 191346,nn4604k). All the insight gained through these projects and the collaboration with all the project partners is gratefully acknowledged. In addition, thanks to Prof. Truls Norby, PhD fellows, and Post Docs, for sharing thoughts, results, and discussions.

Figures and Tables

Table 1. List of the most common nomenclatures for lanthanum tungstate, all referring to the same material. (*$La_{28-x}W_{4+x}O_{54+\delta}$, x=1)

acronym	La/W ratio	1	2	3	4	5
LWO60	6	La_6WO_{12}	3:1 La_2O_3:WO_3	$LaW_{1/6}O_2$	La_6WO_{12}	-
LWO54	5.4	-	-	-	$La_{5.4}WO_{12-\delta}$	$La_{27}W_5O_{55.5}$*
LWO50	5.0	$La_{10}W_2O_{21}$	5:2 La_2O_3:WO_3	-	$La_5WO_{12-\delta}$	-

Table 2. List of the measured density by He-pycnometry as a function of the nominal and measured La/W ratio. The error on the La/W ratio is calculated from the standard deviation of 10 measurements multiplied by 2. The La/W ratio is measured by electron probe microanalysis on specimens sintered at 1500 °C, except LWO60, sintered at 1600 °C. The higher error in composition for LWO60 likely reflects segregation of phases.

acronym	LWO53	LWO54	LWO56	LWO57	LWO60
La/W nominal	5.3	5.4	5.6	5.7	6.0
La/W EPMA	5.30	5.45	5.68	5.75	6.01
$2\sigma_{st}$ (95%)	0.10	0.07	0.08	0.07	0.17
density (g/cm^3)	6.38	6.34	-	6.43	-

Table 3. Summary of the theoretical number of vacancies and tungsten on La(24g) sites (x) as a function of La/W ratio, based on the formula $La_{28-x}W_{4+x}O_{54+\delta}v_{2-\delta}$ (δ=3x/2).

acronym	LWO50	LWO52	LWO53	LWO54	LWO56	LWO57	LWO60	LWO70
La/W nominal	5.0	5.2	5.3	5.4	5.6	5.7	6.0	7.0
x($W_{La}^{\bullet\bullet\bullet}$)	1.33	1.16	1.08	1	0.85	0.78	0.57	0
v	0	0.26	0.38	0.5	0.73	0.84	1.14	2
single phase? (at 1500 °C)	NO	NO	YES	YES	YES	YES	NO	n/a

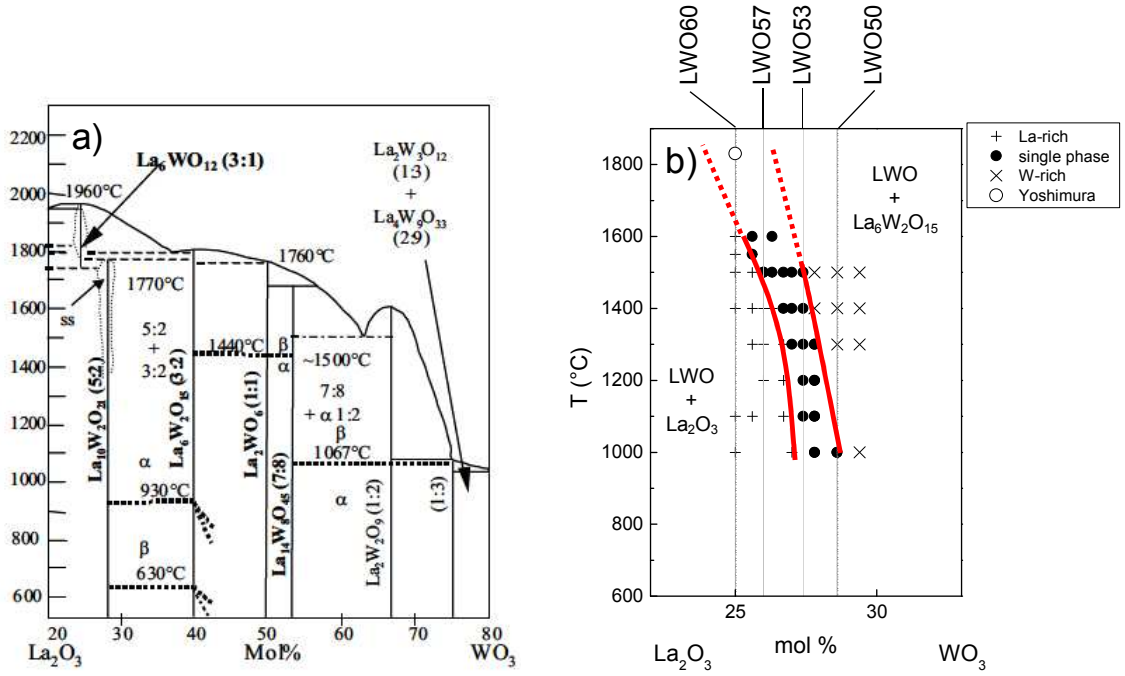

Figure 1. **a)** Phase diagram by Yoshimura and Rouanet [9], re-drawn by Chambrier et al. [14]. **b)** Revised La_2O_3-WO_3 phase diagram based on the data extracted from [13]. The dotted lines have been hypothetically extrapolated.

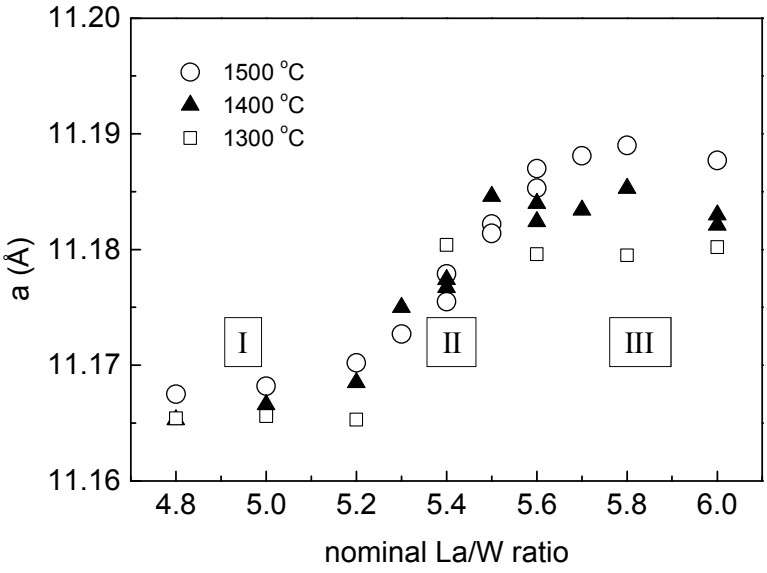

Figure 2. Variation of the lattice parameter obtained by XRD as a function of the nominal La/W ratio after firing at 1300, 1400 or 1500 °C.

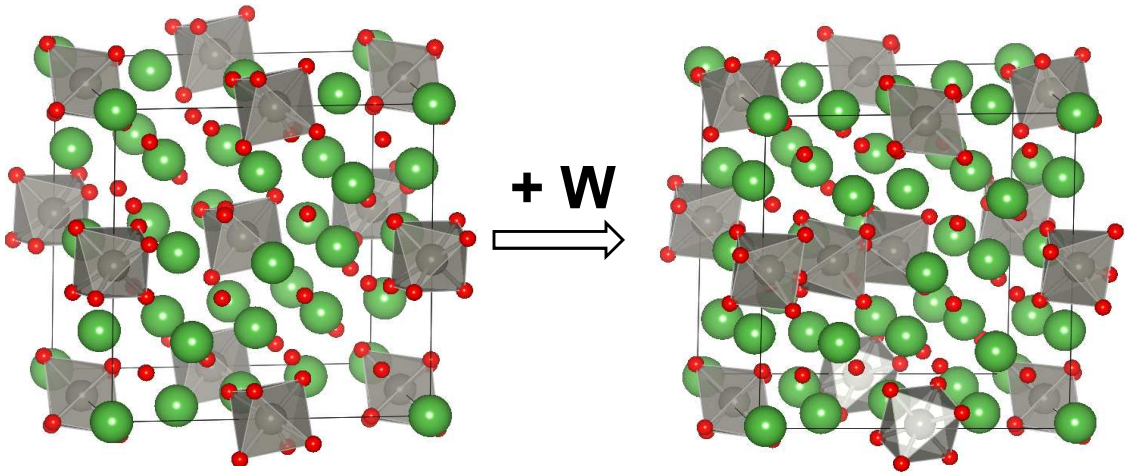

Figure 3. Schematic representation of the local crystal structure of lanthanum tungstate. Left: $La_{28}W_4O_{54}v_2$ ("stoichiometric" composition, not stable). Right: $La_{27}W_5O_{55.5}v_{0.5}$ (one tungsten dissolves in La2(24g) sites to form a stable composition), from ref [19].

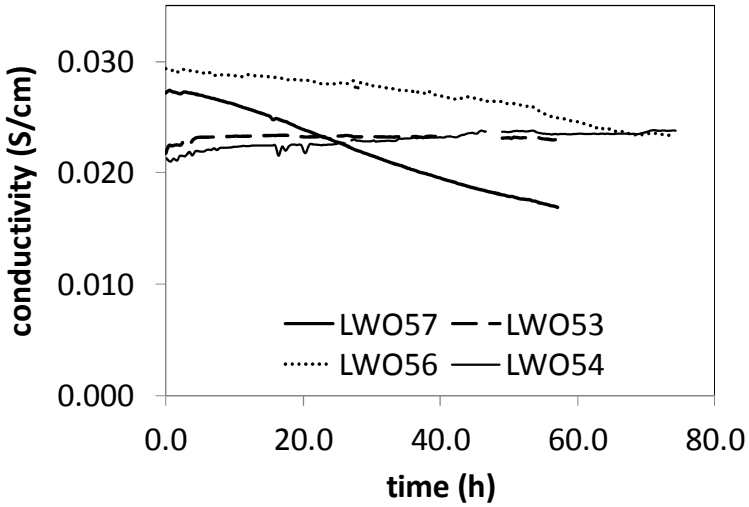

Figure 4. Dependence of the conductivity of different tungstates at 1100 °C under wet H_2.

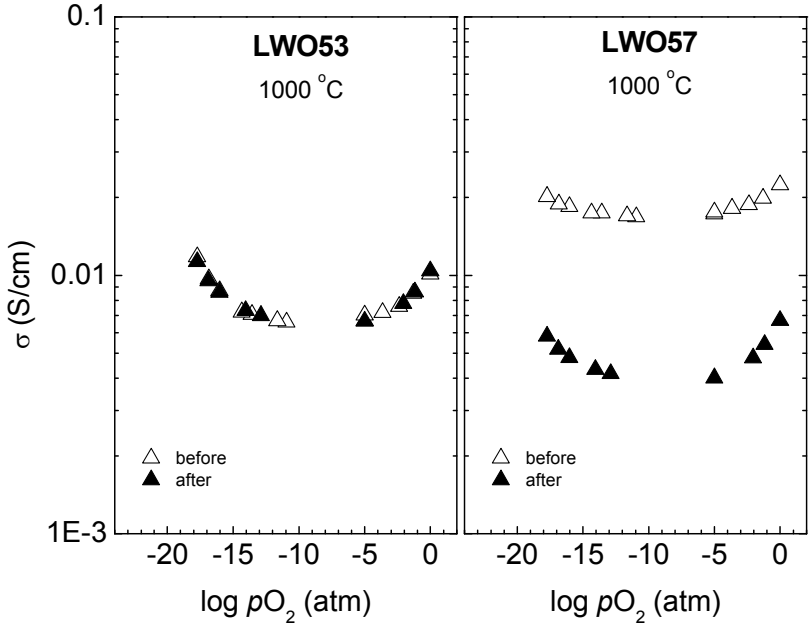

Figure 5. Variation of the total conductivity as a function of oxygen partial pressure at 1000 °C before and after a thermal treatment in wet H_2 at 1100 °C during 60 hours.

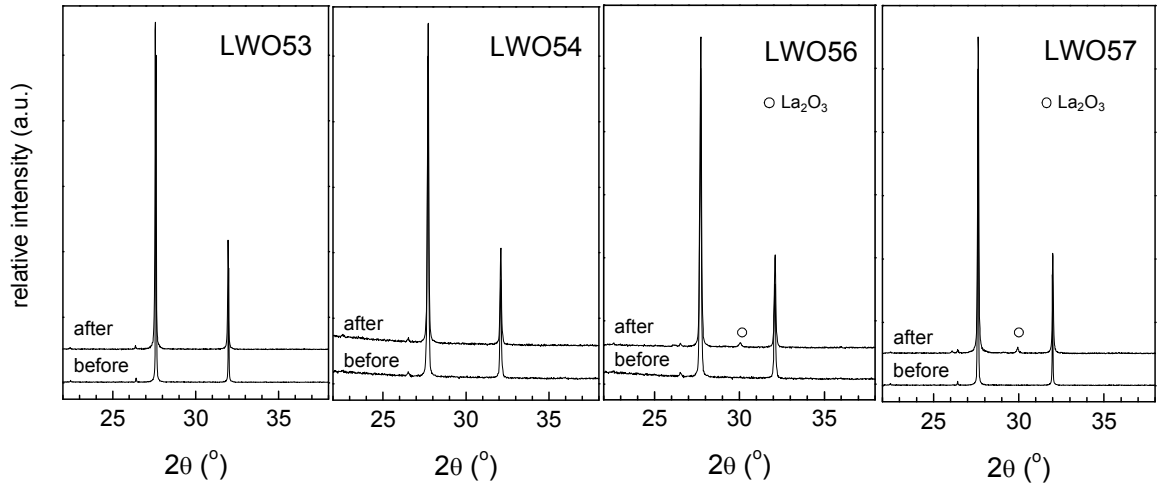

Figure 6. X-ray diffractograms of various LWO compositions before and after long term annealing under reducing conditions at 1100 °C.

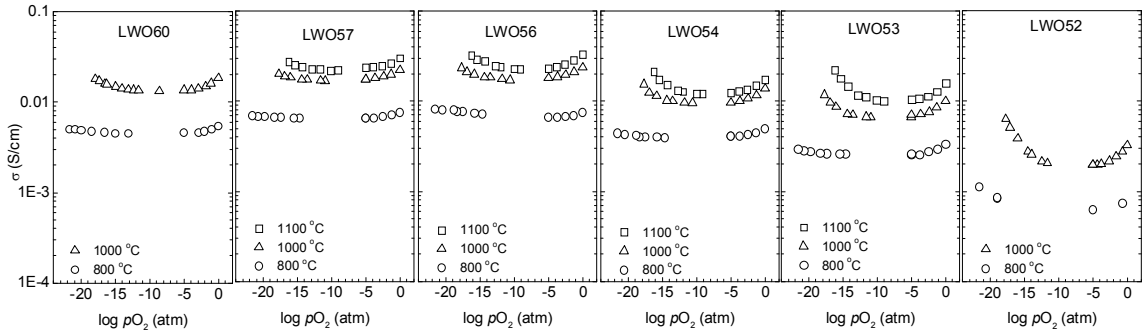

Figure 7. Variation of the total conductivity as a function of oxygen partial pressure at different temperatures from wet H_2 to wet O_2 for decreasing lanthanum content (from left to right) in LWO. All specimens were prepared using the freeze-drying method [13], except LWO60, prepared by solid state chemistry, taken from ref. [28]. Conductivity data is taken from ref. [28] (LWO60) and ref. [29] (for LWO57, LWO54 and LWO53). Additional compositions were measured in parallel experiments.

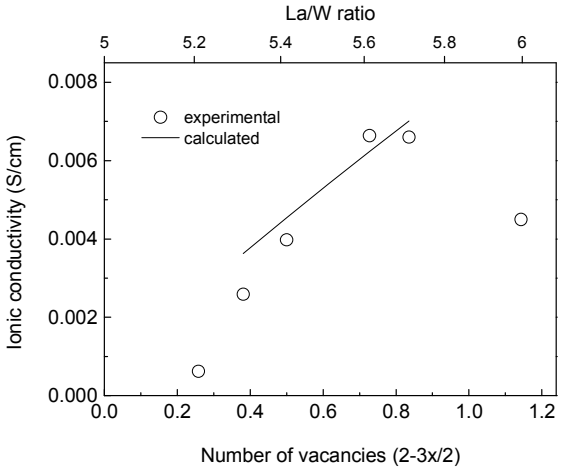

Figure 8. Variation of the experimental ionic conductivity at 800 °C (from **Fig. 7**) as a function of nominal amount of vacancies in $La_{28-x}W_{4+x}O_{54+\delta}v_{2-\delta}$ (**Table 3**), compared to calculated ionic conductivity from the model described in reference [30].

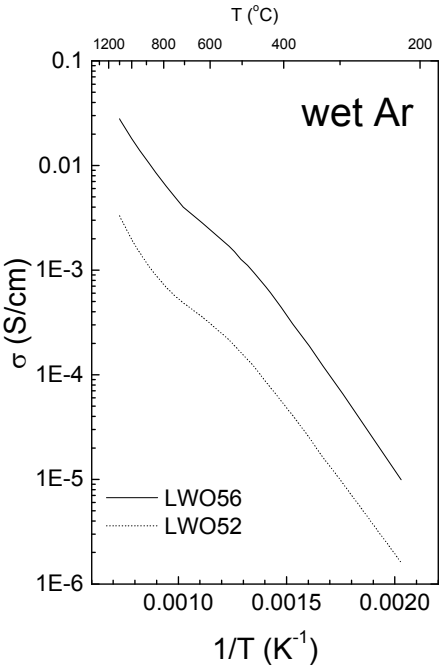

Figure 9. Temperature dependency of the conductivity from 1100 to ~200 °C in wet Ar for LWO56 and LWO52. It mainly reflects ionic conductivity (oxide ion+protonic). Data recorded in parallel with experiments from ref [29].

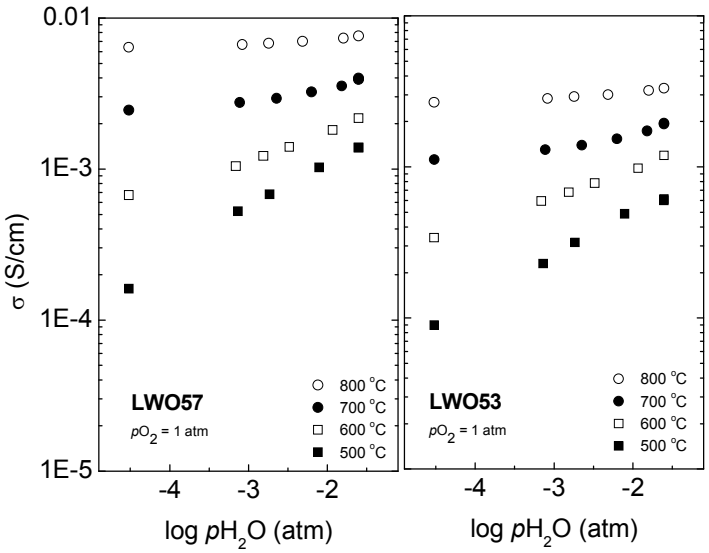

Figure 10. Variation of the total conductivity as a function of water vapour partial pressure in O_2 at different temperatures from 500 to 800 °C for LWO57 [41] and LWO53.

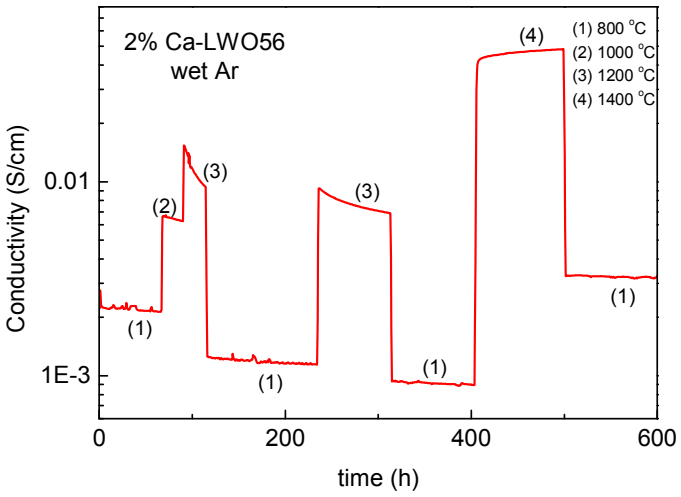

Figure 11. Variation of the conductivity of a 2% Ca-LWO56 in wet Ar over time upon changes in temperature. Measurement recorded after the experiments from ref. [18].

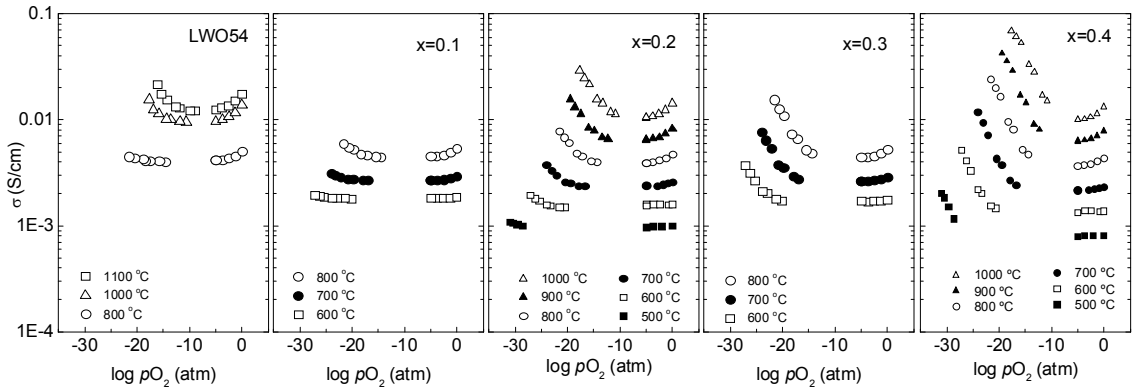

Figure 12. Variation of the total conductivity as a function of oxygen partial pressure at different temperatures for increasing molybdenum content (from left to right). $La_{28-y}(W_{1-x}Mo_x)_{4+y}O_{54+\delta}$ (x=0-0.4), taken from refs [29,30,41].

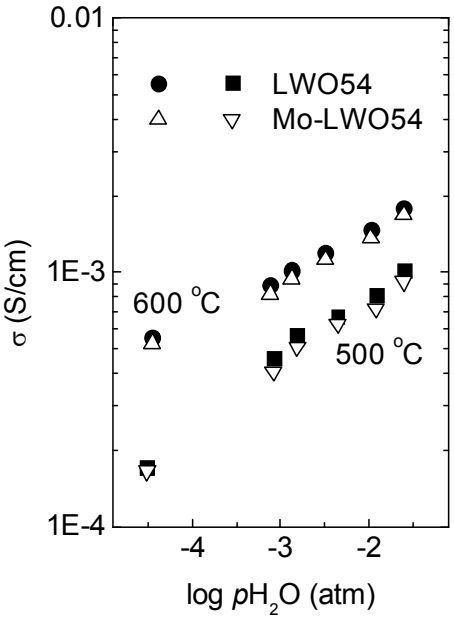

Figure 13. Variation of the total conductivity as a function of water vapour partial pressure in O_2 at 500 and 600 °C for LWO54 and 30% Mo-substituted LWO54, taken from ref. [30].

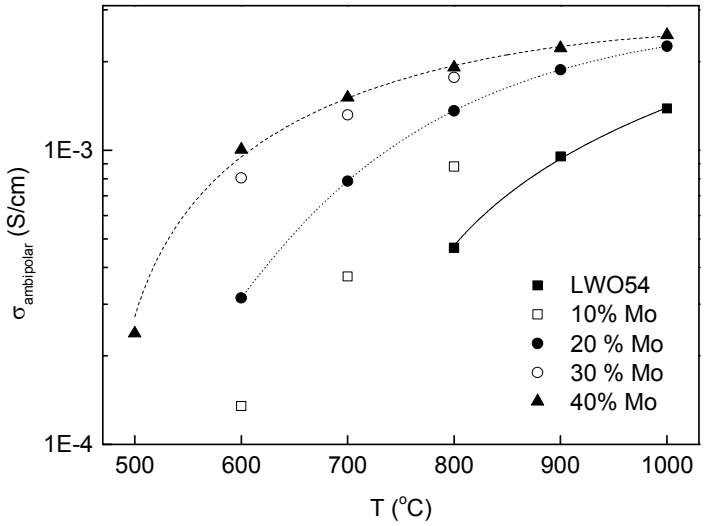

Figure 14. Estimated ambipolar conductivities in wet H_2 of undoped and Mo-substituted LWO. The partial proton conductivities are taken from those obtained using the EMF method (see ref. [30]), which are assumed constant as a function of Mo doping up to 40 % (the author is referred to the text to support this statement). The partial electronic conductivities are extracted from the dependency of the conductivity *vs* pO_2 at each indicated temperature (from [30] and [41]). Lines are guide-for-the-eye purpose, only.

References

[1] S.F. Bartram, Inorg. Chem. 1966, **5(5)**, 749-754.
[2] S. F. Bartram, E. F. Juenke, E. A. Aitken, J. Am. Ceram. Soc. 1964, **47**, 171-175.
[3] E.A. Aitken, S.F. Bartram, E.F. Juenke, Inorg. Chem. 1964, **3(7)**, 949-953.
[4] H. J, Borchardt, Inorg. Chem. 1963, **2(1)**, 170-173.
[5] G.J. McCarthy, R.D. Fisher, G.G. Johnson, C. E. Gooden. "National Bureau of Standards Special Publication, Solid State Chemistry" In Proceedings of the 5th Materials Research Symposium, 1972, 397.
[6] L.L.Y. Chang, M.G. Scroger, B. Phillips, J. Inorg. Nucl. Chem. 1966, **28(5)**, 1179-1184.
[7] L.L.Y. Chang, B. Phillips, Inorg. Chem. 1964, **3(12)**, 1792-1794.
[8] M.M. Ivanova, E.M. Reznik, Izvestiya Akademii Nauk SSSR, Neorganicheskie Materialy, 1972, **8(5)**, 981-983.
[9] M. Yoshimura, A. Rouanet, Mat. Res. Bull. 1976, **11**, 151-158.
[10] T. Hartmann, H. Ehrenberg, G. Miehe, G. Wltschek, H. Fuess, J. Solid State Chemistry 1999, **148**, 220-223.
[11] D. Michel, A. Kahn, Acta Cryst. 1982, **B38**, 1437-1441.
[12] A.P. Richard, D.D. Edwards, J. Sol. St. Chem. 2004, **177**, 2740-2748.
[13] A. Magrasó, C. Frontera, D. Marrero-López, P. Núñez, Dalton Trans. 2009, 10273 – 10283.
[14] M.H. Chambrier, F. Goutenoire, JEEP, EDP Sciences 2009, 00022.
[15] M. Yoshimura, J.F. Baumard, Mat. Res. Bull. 1975, **10(9)**, 983-988.
[16] A. Lashtabeg, J. Bradley, A. Dicks, G. Auchterlonie, J. Drennan, Sol. St. Chem. 2010, **183(5)**, 1095-1101.
[17] C. Solis, S. Escolastico, R. Haugsrud and J. M. Serra, J. Phys. Chem. C, 2011, **115**, 11124-11131.
[18] A. Magrasó, C. H. Hervoches, I. Ahmed, S. Hull, J. Nordström, A. W. B. Skilbred, R. Haugsrud, J. Mater. Chem. A , 2013, **1**, 3774.
[19] A. Magrasó, J. M. Polfus, C. Frontera, J. Canales-Vazquez, L.-E. Kalland, C. H. Hervoches, S. Erdal, R. Hancke, M. S. Islam, T. Norby and R. Haugsrud, J. Mater. Chem., 2012, **22(5)**, 1762–1764.
[20] M. Yoshimura, F. Sibieude, A. Rouanet, M. Foex, J. Solid State Chemistry, 1976, **16(3-4)**, 219-232.
[21] V. K.Trunov, G.I.Tyushevskaya, N.S. Afonskii, Moscow State Univ., Zh. Neorg. Khim., 1968, **13(4)**, 936-939.
[22] G.J. McCarthy, Mat. Res. Bulletin, 1971, **6(1)**, 31-39.
[23] E. Summerville, J. Drennan, D. J. M. Bevan, Le Journal de Physique Colloques, 1977, **38 (C7)**, 73-79.
[24] T. Scherb, S.A.J. Kimber, C. Stephan, P.F. Henry, G. Schumacher, J. Just, S. Escolastico, J.M. Serra, J. Seeger, A.H. Hill, J. Banhart, 2013, arXiv:1305.3385v1.
[25] L.-E. Kalland, A. Magrasó, A. Mancini, C. Tealdi, L. Malavasi, Chem. Mater., 2013, **25 (11)**, 2378–2384.
[26] H. Ehrenberg, T. Hartmann, K. G. Bramnik, G. Miehe and H. Fuess, Solid State Sci., 2004, **6**, 247–250.
[27] T. Shimura, S. Fujimoto, H. Iwahara, Solid State Ionics, 2001, **143**, 117-123.
[28] R. Haugsrud, Solid State Ionics, 2007, **178(7)**, 555-560.

[29] S. Erdal, L.-E. Kalland, R. Hancke, J. Polfus, R. Haugsrud, T. Norby, A. Magrasó, Int. J. Hydrogen Energy, 2012, **37(9)**, 8051-8055.
[30] A. Magrasó, J. Power Sources, 2013, **240**, 583–588.
[31] T. Norby, J. Korean Ceramic Society, 2010, **47**, 19-25.
[32] R. Haugsrud, C. Kjølseth, J. Phys. Chem. Solids, 2008, **69(7)**, 1758-1765.
[33] R. Hancke, A. Magrasó, T. Norby, R. Haugsrud, Solid State Ionics, 2013, **231**, 25–29.
[34] S. Escolástico, C. Solís, J.M. Serra, Solid State Ionics, 2012, **216**, 31-35.
[35] N. Diot, P. Benard-Rocherulle, R. Marchand, Powder Diffraction, 2000, **15(04)**, 220-226.
[36] Nadya Alyeshkina, MSc thesis, "Defects and Transport in Ce-doped $La_{27}W_5O_{55.5}$" (2013) University of Oslo.
[37] Xuemei Cui , MSc thesis "Defects and Transport in Ba-doped $La_{27}W_5O_{55.5}$" (2013) University of Oslo.
[38] W. Xing, K. Toyoura, T. Norby, Int. J. Hydrogen Energy, 2012, **37(9)**, 8062–8065.
[39] M. J. Zayas-Rey, L. dos Santos-Gomez, D. Marrero-Lopez, L. Leon-Reina, J. Canales-Vazquez, M. A. G. Aranda, E. R. Losilla, Chem. Mater., 2013, **25 (3)**, 448–456.
[40] S. Escolastico, J. Seeger, S. Roitsch, M. Ivanova, W.A. Meulenberg, J. Serra, ChemSusChem, 2013, **6(8)**, 1523-1532.
[41] M. Amsif, A. Magrasó, D. Marrero-López, J. C. Ruiz-Morales, J. Canales-Vázquez, P. Núñez, Chem. Mater., 2012, **24 (20)**, 3868–3877.
[42] E. Vøllestad, C.K. Vigen, A. Magrasó, R. Haugsrud, J. Membrane Science, 2014, accepted for publication, DOI: 10.1016/j.memsci.2014.03.011.
[43] R. Haugsrud "New high-temperature proton conductors for fuel cells and gas separation membranes" Handbook of Fuel Cells, 2010.
[44] C. Solis, V. B. Vert, M. Balaguer, S. Escolastico, S. Roitsch, J. M. Serra, ChemSusChem, 2012, **5**, 2155
[45] M. Balaguer, C. Solis, F. Bozza, N. Bonanos, J. M. Serra, J. Mater. Chem. A, 2013, **1(9)**, 3004-3007.
[46] E. Quarez, K.V. Kravchyk, O. Joubert, Solid State Ionics, 2012, **216**, 19-24.
[47] C. Solís, L. Navarrete, S. Roitsch, J.M. Serra, *J. Mater. Chem*., 2012, **22**, 16051.
[48] E. Quarez, Y. Oumellal, O. Joubert, Fuel Cells, 2013, **13(1)**, 34–41.
[49] S. Erdal, PhD thesis "Hydrogen in Oxides: incorporation, transport and effects on electrical properties" University of Oslo, 2011.
[50] V. Gil, J. Gurauskis, C. Kjølseth, K. Wiik, M.-A. Einarsrud, Int. J. Hydrogen Energy, 2013, **38(7)**, 3087-3091.
[51] R. Hancke, S. Fearn, J.A. Kilner, R. Haugsrud, Phys. Chem. Chem. Phys., 2012, **14(40)**, 13971-13978.
[52] E. Vøllestad, T. Norby, R. Haugsrud, Solid State Ionics, 2013, **244**, 57–62.
[53] E. Quarez, K.V. Kravchyk, O. Joubert, Solid State Ionics, 2012, **216**, 19-24.
[54] T. Norby, R. Haugsrud, "Dense ceramic membranes for hydrogen separation. I: Nonporous Inorganic Membranes for Chemical Processing". Wiley-VCH Verlagsgesellschaft 2006 ISBN 3-527-31342-7. p. 1-48.
[55] S.-J. Song, E.D. Wachsman, J. Rhodes, S.E. Dorris, U. Balachandran, "Numerical modeling of hydrogen permeation in chemical potential gradients" Solid State Ionics, 2003, **164**, 107–116.
[56] X. Qi, Y.S. Lin, Solid State Ionics, 2000, **130**, 149–156.
[57]G.C. Mather, M.S. Islam, Chem. Mater., 2005, **17**, 1736-1744.
[58] T. Oh, H. Yoon, E.D. Wachsman, Solid State Ionics, 2009, **180**, 1233–1239.

[59] S. Hamakawa, L. Li, A. Li, E. Iglesia, Solid State Ionics, 2002, **148**, 71-81.
[60] S. Cheng, V.K. Gupta, J.Y.S. Lin, Solid State Ionics, 2005, **176**, 2653–2662.
[61] J. Li, H. Yoon, E.D. Wachsman, J. Membrane Science, 2011, **381**, 126-131.

The structural and functional properties of proton conducting lanthanum tungstate, $La_{28x}W_{4+x}O_{54+3x/2}$ ($x = 1$), are reviewed.